Mapping ErbB receptors on breast cancer cell membranes during signal transduction

Shujie Yang[1,*], Mary Ann Raymond-Stintz[1,*], Wenxia Ying[2], Jun Zhang[3], Diane S. Lidke[1], Stanly L. Steinberg[2], Lance Williams[3], Janet M. Oliver[1] and Bridget S. Wilson[1,‡]

[1]Department of Pathology and Cancer Research and Treatment Center, [2]Department of Mathematics and Statistics and [3]Department of Computer Science, University of New Mexico, Albuquerque, NM 87131, USA

*These authors contributed equally to this work
‡Author for correspondence (e-mail: bwilson@salud.unm.edu)

Accepted 12 June 2007
Journal of Cell Science 120, 2763-2773 Published by The Company of Biologists 2007
doi:10.1242/jcs.007658

Summary

Distributions of ErbB receptors on membranes of SKBR3 breast cancer cells were mapped by immunoelectron microscopy. The most abundant receptor, ErbB2, is phosphorylated, clustered and active. Kinase inhibitors ablate ErbB2 phosphorylation without dispersing clusters. Modest co-clustering of ErbB2 and EGFR, even after EGF treatment, suggests that both are predominantly involved in homointeractions. Heregulin leads to dramatic clusters of ErbB3 that contain some ErbB2 and EGFR and abundant PI 3-kinase. Other docking proteins, such as Shc and STAT5, respond differently to receptor activation. Levels of Shc at the membrane increase two- to five-fold with EGF, whereas pre-associated STAT5 becomes strongly phosphorylated. These data suggest that the distinct topography of receptors and their docking partners modulates signaling activities.

Supplementary material available online at
http://jcs.biologists.org/cgi/content/full/120/16/2763/DC1

Key words: ErbB, Microdomains, Shc, PI 3-kinase, STAT5

Introduction

The ErbB family consists of four related receptors, ErbB1 (EGFR/Her1), ErbB2 (Neu/Her2), ErbB3 and ErbB4 (Warren and Landgraf, 2006; Yarden and Sliwkowski, 2001). These receptors are single-pass transmembrane proteins with an extracellular ligand binding domain and a cytoplasmic tail containing an integral tyrosine kinase domain and multiple tyrosine phosphorylation sites. Upon ligand binding, the ErbB receptors form homo- or heterodimers that are trans-phosphorylated by their active kinase domains. Exceptions are ErbB3, which has very poor kinase activity, and ErbB2, which does not bind ligands. Once phosphorylated, all of the ErbB receptors serve as docking sites for the recruitment of cytoplasmic adaptor proteins and enzymes, initiating signaling cascades that control multiple cellular processes.

Mutations, gene amplifications and protein overexpression of ErbB family members are all linked to carcinogenesis (Roskoski, Jr, 2004). In particular, ErbB2 is overexpressed in ~30% of all breast cancers and is correlated with poor prognosis (DiGiovanna et al., 2005; Kraus et al., 1987). Importantly, the cooperative interplay between multiple ErbB family members profoundly influences neoplastic transformation and survival (Alimandi et al., 1995; Harari and Yarden, 2000; Tikhomirov and Carpenter, 2004). Current models suggest that ErbB2 is the preferred heterodimerizing partner for other ErbBs, with relatively poor homodimerizing capabilities. This is particularly intriguing on the basis of recent structural studies of ErbB receptors (Burgess et al., 2003). The extracellular domains of EGFR, ErbB3 and ErbB4 have a closed conformation that unfolds upon ligand binding (Bouyain et al., 2005; Burgess et al., 2003). Because ErbB2 constitutively assumes an open conformation, it seems possible that ErbB2 needs to be sequestered from other copies of itself – or from the ligand-binding ErbBs – to prevent premature signaling. In light of this complexity, the development and use of new, specific therapies tailored to inhibit ErbB targets present both opportunity and challenge (Rowinsky, 2004).

Signal transduction through ErbB receptors begins at the plasma membrane. Many studies implicate membrane microdomains (lipid rafts, membrane rafts) in signaling via EGFR and other receptors with integral tyrosine kinase activity. Anderson and co-workers provided early evidence that EGF receptors localize to caveolae, considered by many to be a specialized lipid raft structure (Smart et al., 1995). According to one model, the EGFR moves out of caveolae following stimulation with EGF (Mineo et al., 1999). Other work has suggested that non-caveolar lipid rafts sequester EGF receptors, influence their dimerizing and ligand binding properties or mediate endocytosis (Nagy et al., 2002; Pike et al., 2005; Puri et al., 2005; Ringerike et al., 2002; Roepstorff et al., 2002). Sophisticated fluorescence imaging techniques have documented the large-scale clustering of ErbB receptors (Ichinose et al., 2004; Nagy et al., 1999) and demonstrated that EGFR exhibits more restricted diffusion than ErbB2 (Orr et al., 2005). These diverse findings point to the need to better understand the nanoscale relationships of ErbB receptors in the membranes of normal and malignant cells.

Immunoelectron microscopy of native membrane sheets has proven to be a powerful technique for mapping the dynamic behavior of activated FcεRI and BCR, two tyrosine kinase-linked immunoreceptors (Kim et al., 2005; Wilson et al., 2000; Wilson et al., 2001; Wilson et al., 2004). Immunoelectron microscopy has also been applied to the study of Ras isoforms, demonstrating the distinct membrane localization properties of

H-Ras and K-Ras (Prior et al., 2003). In the present study, we apply this method to map the topography of ErbB receptors and several of their signaling partners in cultured SKBR3 breast cancer cells. Our results show distinct patterns of membrane clustering for the different ErbBs. They also reveal distinct recruitment behavior and topographical relationships of ErbBs for different signaling adaptors and enzymes.

Results

ErbBs cluster when expressed individually in transfected CHO cells

We began this study by establishing the clustering behavior of ErbB receptor in the absence of expression of other ErbBs. We used stably transfected CHO cells that lack endogenous EGFR or ErbB3 and have only minute amounts of endogenous ErbB2. Transfectants expressing visible fluorescent-protein chimeras of ErbB2 and ErbB3 were flow-sorted to enrich in cells expressing either high or low numbers of each receptor on the cell surface. The $CHO^{EGFR\text{-}GFP}$ cell line was clonally derived and not amenable to flow sorting.

Results in supplementary material Fig. S1A show membrane sheets prepared from resting $CHO^{EGFR\text{-}GFP}$ cells and labeled from the outside with GR15 anti-EGFR antibodies, followed by 5-nm gold-conjugated secondary antibodies. A coated pit, lacking gold label, is marked with an arrow. This image shows that EGFR is preclustered. The inset in supplementary material Fig. S1 confirms the clustered state of receptors using the Hopkins statistical test for random distributions (Wilson et al., 2004). There were low levels of EGFR tyrosine phosphorylation in resting cells; as expected, EGF (20 nM) led to a rapid increase in phosphorylation (see supplementary material Fig. S1I). However, addition of EGF to transfected CHO cells did not markedly change EGFR cluster size (supplementary material Fig. S1B). All results were confirmed by the Hopkins test (insets).

Previous work using the immunogold technique has demonstrated that labeling efficiency rarely approaches 100%. We find that labeling with small gold probes (3-5 nm) typically yields the best results, whereas labeling with larger probes (10 nm) is markedly less efficient. In double labeling procedures (see Figs 2-5), experiments are typically repeated by reversing the sizes of gold to validate co-clustering results. In single labeling procedures, we optimize results by using only small gold probes. In both cases, it is useful to apply computer simulation methods to reconstruct complete data from incomplete data sets. Fig. S1C shows results of applying Hidden Markov Random Field modeling (Zhang et al., 2007) to simulate the complete distribution of EGFR on the surface of transfected $CHO^{EGFR\text{-}GFP}$ cells. This image corrects mathematically and spatially for underlabeling. Assuming 80,000 EGFR per cell, we estimated that 39% and 54% of the EGFR were labeled with 5 nm anti-EGFR gold particles before and after EGF, respectively. The predicted average size of EGFR clusters on the surface of SKBR3 cells is about seven receptors, although the sizes ranged from singlets to as many as 80 receptors. We found no significant difference in cluster size before and after activation with EGF.

ErbB3 and ErB2 are also found in small clusters on the surface of transfected CHO cells. Following flow sorting, we compared the average cluster size on cells expressing low (supplementary material Fig. S1D) and high (supplementary material Fig. S1E,F) levels of ErbB3 or low (supplementary material Fig. S1G) and high (supplementary material Fig. S1H) levels of ErbB2. Samples of the sorted cells were also lysed and solubilized proteins were separated by SDS-PAGE, followed by immunoblotting with anti-ErbB3 or anti-ErbB2 antibodies (supplementary material Fig. S1J,K). Results in supplementary material Fig. S1D,E show that ErbB3 cluster size on the surface of resting CHO cells is largely independent of expression levels. Remarkably, the addition of heregulin (also known as neuregulin 1) leads to formation of significantly larger ErbB3 clusters on the CHO surface (supplementary material Fig. S1F). Consistent with neglible kinase activity of ErbB3 (Guy et al., 1994; Sierke et al., 1997), overexpression alone results in barely detectable phosphorylation of the ErbB3 cytoplasmic tail at Tyr1289 (supplementary material Fig. S1J). Addition of heregulin to $CHO^{ErbB3\text{-}mCit}$ cells also results in a very slight increase in ErbB3 Tyr phosphorylation (not shown). This might be explained if, as proposed in one early report (Guy et al., 1994), ErbB3 is only a poor kinase and not a completely dead kinase. Alternatively, the very low endogenous expression of ErbB2 may support small amounts of kinase-competent ErbB3-ErbB2 heterodimers.

In contrast to the other family members, ErbB2 has no known ligand. We noted that, although most clusters in CHO cells overexpressing ErbB2-mYFP remain small, occasional very large clusters containing 50-100 gold particles are observed. In addition, analysis of ErbB2 in a population flow-sorted for high expressors showed that overexpression alone leads to substantial ErbB2 Tyr phosphorylation, demonstrated using anti-PY1248 antibodies in Figure S1K. This result is consistent with the concept that high levels of receptors override the relatively poor homodimerizing capabilities of ErbB2 (Garrett et al., 2003; Penuel et al., 2002), leading to productive and active homodimers.

Limited colocalization of endogenously expressed ErbBs in breast cancer cell membranes

Having established that each of the three ErbB receptors inherently cluster on CHO cells, we turned to a cancer relevant cell model system where multiple family members are co-expressed. We chose the SKBR3 breast cancer cell line, that has exceptionally high levels of endogenous ErbB2 (>2,750,000 molecules per cell), intermediate levels of EGFR (<200,000 molecules per cell) and modest levels of ErbB3 (<70,000 molecules per cell). ErbB4 is undetectable in this cell line. These values were determined by quantitative flow cytometry (not shown) and confirmed by western blotting (Fig. 1E). Biochemical studies, reported in Fig. 1A, established high basal levels of ErbB2 phosphorylation and some detectable ErbB3 phosphorylation, even after serum starvation. As expected, EGF led to EGFR phosphorylation (Fig. 1A) and an increase in EGFR kinase activity (Fig. 1B, left), but produced little change in ErbB3 phosphorylation. Although a change in ErbB2 phosphorylation was barely detectable after EGF addition (see Fig. 1D), there was a transient increase in kinase activity associated with ErbB2 immunoprecipitates at 1 min of EGF treatment (Fig. 1B, right).

Results in Fig. 1C show the effects of putative EGFR-selective inhibitors (AG1478, PD153035, Iressa) and ErbB2-selective inhibitors (AG879) on in vitro kinase activity. The same drugs are tested for effects on EGF- and heregulin-

stimulated tyrosine phosphorylation in intact cells in supplementary material Fig. S2. In general, higher concentrations were required to inhibit phosphorylation in culture than in the in vitro kinase assay, presumably due to limited cellular uptake of the drugs. EGFR and ErbB3 were highly sensitive to AG1478 and ErbB2 was particularly sensitive to AG879. Continuing studies used a combination of AG1478 and AG879 to ablate phosphorylation of all three receptors.

A co-immunoprecipitation assay was performed, using NP-40 detergent lysates, as a biochemical method to evaluate heterodimerization between the ErbB family members in SKBR3 cells. Fig. 1D shows that this method yields data that are difficult to interpret. For example, ErbB1 immune complexes contain significant amounts of ErbB2 (and very little ErbB3). This may reflect pre-formed dimers, because the amount of ErbB2 co-precipitating does not change with EGF treatment, or that the dimers form after membrane lysis. By contrast, when the experiment was performed in reverse by immunoprecipitating ErbB2, the immune complexes contained barely detectible ErbB1 or ErbB3. ErbB3 immune complexes contain a small amount of ErbB2 and essentially no ErbB1. In this experiment, probing of immune complexes with anti-phosphotyrosine antibodies detects ligand-dependent activation of ErbB1 and ErbB3 (Fig. 1D, top panel). The double band detected by PY20 blotting of ErbB1 precipitates is consistent with co-precipitation of ErbB2, that migrates slightly slower in SDS-PAGE than ErbB1. We can conclude that some ErbB1/ErbB2 heterodimers do occur. However, the reliability of measuring dimerization by immunoprecipitation depends strongly on the antibodies used and can be markedly impacted by the choice of detergent. Based upon these results, we chose to use double labeling protocols on native membrane sheets to evaluate the proximity of ErbB family members, before and after ligand addition (see Fig. 3, below).

Limited colocalization of endogenously expressed ErbBs in breast cancer cell membranes

We first examined the clustering state of ErbB2 on SKBR3 cells. As predicted from the work of Lisanti and co-workers

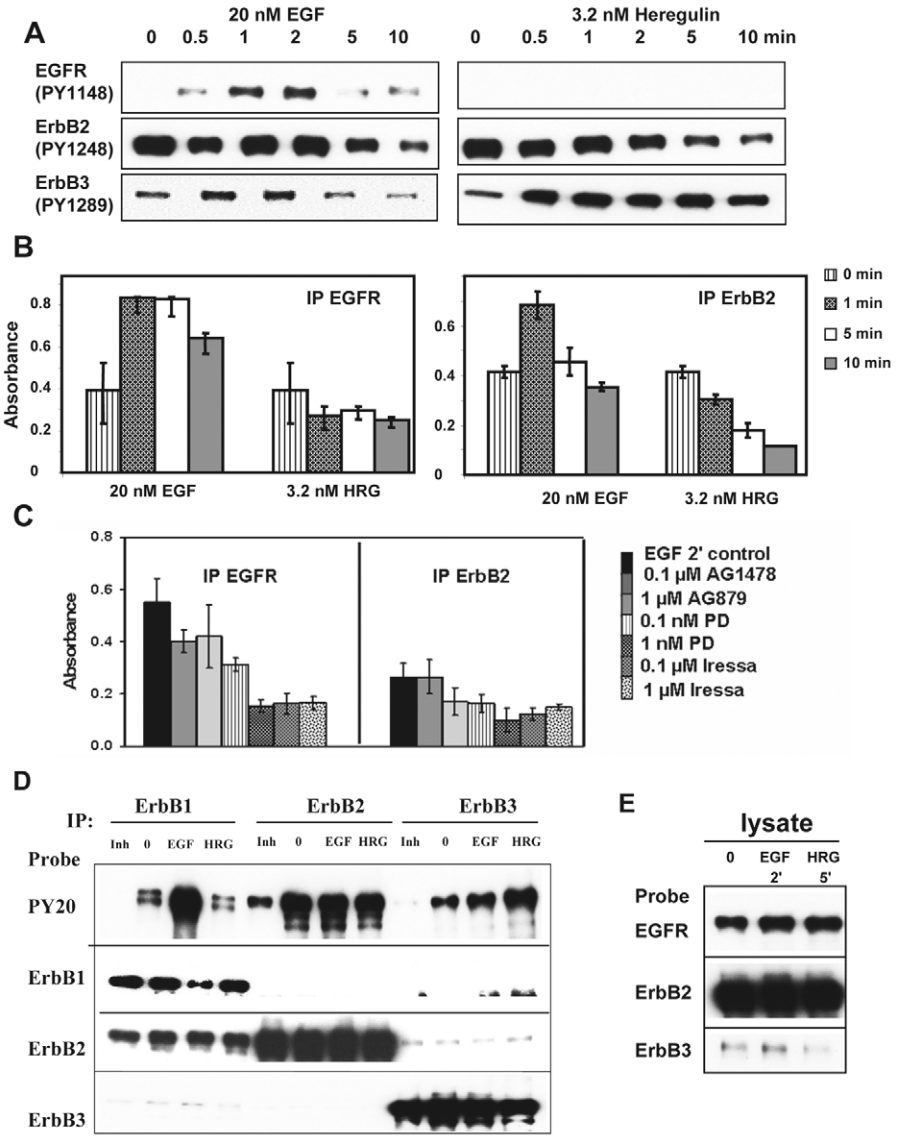

Fig. 1. Biochemical analysis of endogenous ErbB family members in SKBR3 cells. (A) Tyrosine phosphorylation status of ErbB receptors in SKBR3 cells after 2 hours serum starvation (0) or after indicated time course of treatment with either EGF (20 nM) or heregulin (3.2 nM). (B) Kinase activity associated with EGFR or ErbB2 immunoprecipitates prepared from resting, EGF- or heregulin-treated cells, measured in vitro by K-LISA. (C) Effects of kinase inhibitors on EGFR or ErbB2 kinase activity, measured by K-LISA in immunoprecipitates prepared from cell lysates after a 2-minute stimulus with 20 nM EGF. K-LISA values are corrected for baseline color development typical in IgG controls. (D) Co-precipitation assay for ErbB heterodimerization. Where indicated, cells were stimulated with 20 nM EGF or 3.2 nM heregulin, followed by lysis with 1% NP-40 and immunoprecipitation using EGRF-, ErbB2- or ErbB3-specific antibodies. Samples were subjected to SDS-PAGE, followed by immunoblotting with ErbB-specific antibodies. (E). Immunoblotting of equal amount of SKBR3 lysates (10 μg of protein each lane) to document the relative levels of all three ErbB3 family members.

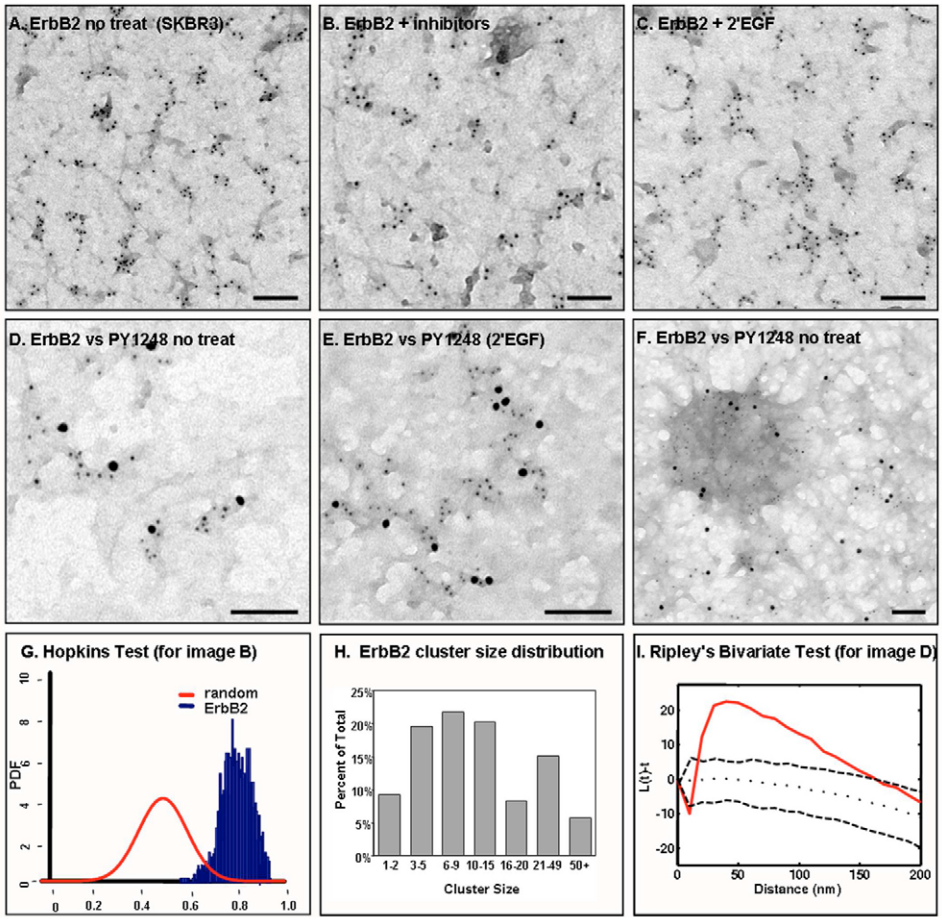

Fig. 2. ErbB2 clustering in SKBR3 cells. (A-F) Membrane sheets were prepared from serum-starved cells (A,D,F), from cells pretreated with the combination of 1 μM AG1478 + 20 μM AG879 for 2 hours (B), or from cells that were serum starved, then stimulated with 20 nM EGF for 2 minutes (C,E). Distributions of ErbB2 were determined by immunogold labeling from the inside using RB9040 primary antibodies and 5-nm-gold-conjugated secondary antibodies. In D-F, membranes were also double labeled with 10-nm-gold reagents to detect phosphorylated tyrosine 1248 in the ErbB2 cytoplasmic tail. (G) Hopkins test is positive for ErbB2 clustering (applied to the data from image A). (H) Range of cluster size for resting ErbB2 in five images from the same experiment in 2A. (I) Positive Ripley's test for coincidence of label for pan-specific anti-ErbB2 antibodies vs phospho-specific ErbB2 antibodies. Bars, 0.1 μm.

(Koleske et al., 1995), these highly transformed cells have few or no caveolae. Like high expressor CHO cells, the surface of serum-starved SKBR3 is studded with ErbB2 clusters (Fig. 2A). ErbB2 cluster size proved remarkably refractory to interventions. Cluster size does not change after 1 hour treatment with AG1478 and AG879 to block ErbB2 phosphorylation (Fig. 2B). ErbB2 cluster size also does not change after the addition of EGF that would be predicted to initiate the formation of both EGFR homodimers and EGFR/ErbB2 heterodimers (Fig. 2C). Results in Fig. 2D-F show membrane sheets that were double labeled for ErbB2 and phosphorylated ErbB2 (PY1248). All of the ErbB2 clusters in serum-starved cells contain label that mark the presence of phosphorylated receptor and there is little or no change after the addition of EGF (Fig. 2E). Based upon Markov Random Field simulations that account for underlabeling in the EM approach (demonstrated in supplementary material Fig. S1C), we estimate that the average ErbB2 cluster contains about nine receptors. In the lower panel of this figure, we document the multiple spatial statistics approaches we used to confirm these visual impressions. Fig. 2G shows the application of the Hopkins test used to prove that ErbB2 distribution in Fig. 2A is significantly non-random. Fig. 2H shows the full range of ErbB2 cluster sizes in a group of five images from the same experiment as Fig. 2A (resting cells). Like CHO cells, resting SKBR3 cells have occasional very large ErbB2 clusters with over 50 particles (last bar, Fig. 2H); these very large clusters do not contain a higher ratio of phosphorylated receptor (Fig. 2F). Fig. 2I shows the application of the Ripley's bivariate test to show that the labels for ErbB2 and phospho-ErbB2 are statistically co-clustered. Thus, although ErbB2 clusters in SKBR3 cells all contain a significant fraction of phosphorylated, active ErbB2, the driving force for cluster formation is clearly not its phosphorylation state.

A central goal was to determine if these three family members behave in a coordinated or independent manner, when they are expressed together in the cancer cell. In Fig. 3, membrane sheets were double labeled for ErbB2 versus EGFR or ErbB3, with and without their ligands. Fig. 3A shows that SKBR3 cells generally maintain distinct clusters of ErbB2 and EGFR (arrows) before the addition of EGF, although occasional co-clusters can be observed (encircled). This image fails the Ripley's statistical test for co-clustering (supplementary material Fig. S3). Furthermore, of 6 images analyzed from this data set, only one passed the Ripley's co-clustering test.

Fig. 3B shows the results of double labeling membrane sheets from cells stimulated for 2 minutes with EGF. This image weakly passes the Ripley's test for co-clustering (supplementary material Fig. S3), which is explained by two prominent co-clusters (encircled in Fig. 3B) as well as many segregated clusters containing only EGFR or ErbB2 alone. Segregation of the two receptor clusters was more prominent than mixing, because only 30% of the images passed the Ripley's test for co-clustering in the EGF-treated data set. We

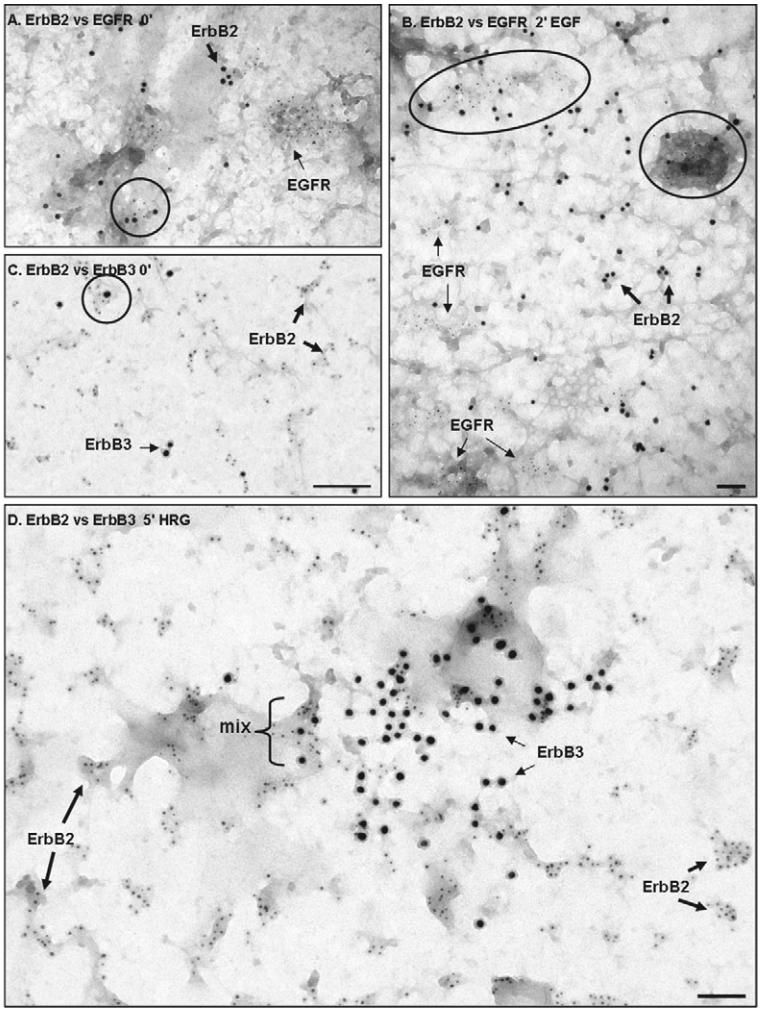

Fig. 3. Analysis of ErbB2 co-clustering with EGFR and ErbB3 in SKBR3 cells. (A-D) Membrane sheets were prepared from serum-starved cells (A,C) or from cells that were serum starved and then stimulated with either 20 nM EGF for 2 minutes (B) or 3.2 nM heregulin for 5 minutes (D). Sheets in A and B were double labeled from the inside with antibodies to ErbB2 (10-nm gold) and EGFR (5-nm gold); Sheets in C and D were double labeled from the inside for ErbB2 (5-nm gold) and ErB3 (10-nm gold). Circles in A-C, as well as the bracket in D, indicate co-clusters of ErbB2 with either EGFR or ErbB3. Labeled arrows point to clusters containing only a single species of ErbB receptor. Bars, 0.1 μm.

speculate that the distinct spatial distributions reflect low amounts of EGF-induced heterodimerization.

Fig. 3C shows that most ErbB2 and ErbB3 also cluster independently in resting cells (arrows), with occasional co-clusters (encircled in Fig. 3C). Only one of five images passed the Ripley's co-clustering test. The most striking result, however, is the dramatic clustering of ErbB3 after 5 minutes treatment with heregulin (Fig. 3D). In this image, the large gold particles marking ErbB3 form a large, dispersed cluster that is over 400 nm wide. Small gold particles marking ErbB2 span the entire membrane sheet (bold arrows), with some of these clusters falling within the larger ErbB3 cluster (bracket). It is important to note that the EM assay establishes only proximity and is not a direct measure of dimerization. However, these 'mixed clusters' indicate the opportunity for heterodimers of ErbB2 and ErbB3 to form. Furthermore, the mixing is of sufficient magnitude to pass the Ripley's test for co-clustering (see supplementary material Fig. S3). Because of the wide distribution of ErbB2, the impression from these experiments is that ErbB2 is neither excluded nor specifically recruited to the ErbB3 patch. It appears that, with 2.7 million ErbB2 receptors, abundance alone is sufficient to ensure that the large ErbB3 patches will contain some ErbB2.

We also evaluated membranes double-labeled for EGFR and ErbB3. We found very little co-clustering in resting membranes (not shown). We found the large ErbB3 clusters induced by heregulin do have some EGFR interspersed through the cluster. However, these images fail the Ripley's test for co-clustering. A representative micrograph, along with the Ripley's analysis, is shown in supplementary material Fig. S4. Thus, although there is also potential for ErbB3-EGFR heterodimers in these clusters, it appears that ErbB3 clusters also do not specifically recruit EGFR.

Three downstream signaling molecules – Shc, PI 3-kinase and STAT5 – have distinct recruitment behavior and topographical relationships to ErbBs

It is well established that specific phosphotyrosines in the cytoplasmic tails recruit cytoplasmic adaptors and downstream effectors to active ErbB receptors (Jorissen et al., 2003). The general model is that these proteins reside in the cytoplasm and are recruited to the membrane following phosphorylation of specific tyrosine on receptor tails. Here, we evaluated the spatial and kinetic relationships of three of these proteins, Shc, PI 3-kinase and STAT5, with the membrane and with the individual ErbB receptors, generating evidence for distinct recruitment behaviors for the different signaling proteins.

Fig. 4 reports results of experiments directed at Shc, an adaptor that binds strongly to EGFR phosphopeptides (Schulze et al., 2005). When evaluated in vitro, Shc is also capable of binding phosphopeptides derived from the ErbB2 tail (Schulze et al., 2005). Simple cell fractionation experiments revealed the presence of two isoforms of Shc in crude cytosol and membrane fractions from SKBR3 cells (Fig. 4A). The smaller p46 isoform of Shc was primarily cytosolic regardless of treatment. By contrast, resting membranes contained significant amounts of the larger p52 isoform of Shc (Shc-p52). Shc-p52 membrane association was reduced by treatment with tyrosine kinase inhibitors and increased by incubation with EGF. Cytosolic Shc-p52 was correspondingly increased by tyrosine kinase inhibitors and reduced by incubation with EGF. In comparison with EGF, heregulin caused a smaller loss of cytosolic Shc-p52 and a correspondingly modest gain in membrane-associated Shc-p52. The electron micrographs in Fig. 4B,C confirm the recruitment of Shc to plasma membranes of EGF-treated cells.

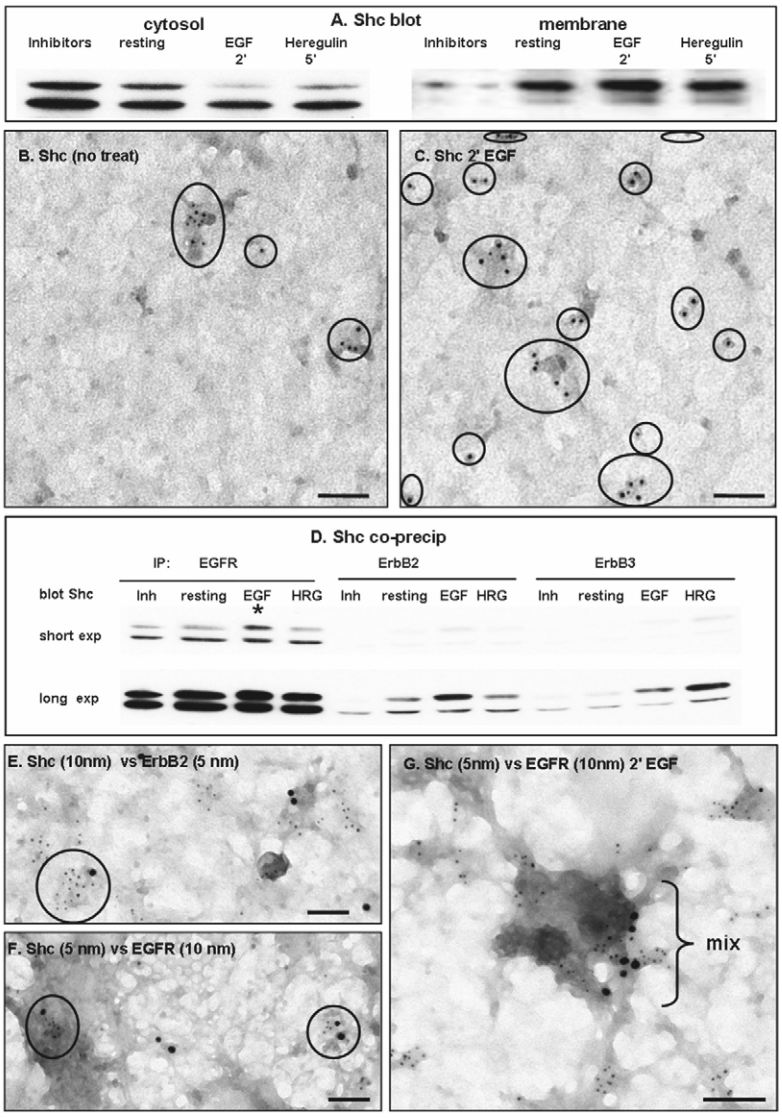

Fig. 4. Membrane recruitment of Shc following EGF treatment. (A) SKBR3 cells were serum starved (resting), treated for 1 hour with a combination of 1 μM AG1478 + 20 μM AG879, or serum starved and stimulated for 2 minutes with 20 nM EGF or 5 minutes with 3.2 nM heregulin, followed by fractionation to yield crude cytosol and membrane fractions. Samples were subjected to SDS-PAGE and immunoblotting with pan-reactive anti-Shc antibodies. (B,C,E-G) Membrane sheets were prepared from serum starved cells (B,E,F) or EGF-simulated cells (C,G) and either singly labeled with 5 nm gold reagents recognizing Shc or double labeled for Shc and either ErbB2 or EGFR, as indicated by labels on each image. Circles in B,C highlight singly-labeled clusters of Shc in these membranes. Circles in E and F show co-clusters of Shc with ErbB2 or EGFR in serum-starved cells. Bracket in G indicates co-cluster of Shc with EGFR after a 2-minute EGF treatment. (D). Immunoblotting evidence for the co-precipitation of Shc with EGFR and, to a much lesser extent, with ErbB2 and ErbB3. Treatment of cells is indicated. Bars, 0.1 μm.

For the experiment shown here, the average number of gold particles marking Shc in resting cells was 15 per μm^2 (Fig. 4B, encircled). After 2 minutes of EGF treatment, this increased fourfold to an average of 70 gold particles per μm^2 (Fig. 4C, encircled; plot in supplementary material Fig. S3). When evaluated in multiple experiments, we routinely found two- to five-fold increases in Shc at the membrane of EGF-treated cells.

The association of Shc with ErbB isoforms is presented in Fig. 4D-G. A significant amount of Shc-p52 co-precipitates with EGFR from resting and inhibitor-treated cells (Fig. 4D). EGF treatment causes a marked increase in the association of Shc-p52 with EGFR. This recruitment is readily observed on short exposure of the blot to film (marked with an asterisk in Fig. 4D). Longer exposure of the blot to film permits detection of additional Shc association with the very abundant ErbB2 (again with an increase in Shc-p52 bound after EGF treatment) and with ErbB3 (with an increase in Shc-p52 bound after heregulin or EGF treatment). In Fig. 4D, anti-ErbB immunoprecipitates also contain the smaller p46 isoform of Shc, in amounts that are relatively unaffected by treatment conditions. Since Shc-p46 is primarily cytosolic (Fig. 4A), we speculate that this Shc-p46 may have bound to receptor tails following the lysis procedure, creating an appearance of co-association that is not supported by independent methods.

Experiments with membrane sheets confirmed the co-clustering of Shc with ErbB2 (Fig. 4E) and EGFR (Fig. 4F) in membranes prepared from serum-starved cells. Shc-EGFR co-clustering and adjacency of the co-clusters to coated pits were both prominent features of EGF-activated membranes (Fig. 4G). This is consistent with work by Sorkin and co-workers (Huang et al., 2004) and others showing that EGFR is predominantly taken up by clathrin-mediated endocytosis. When evaluated by the Ripley's co-clustering test, a majority of images from both resting and activated cells passed the test for colocalization of activated EGFR with Shc (see example in supplementary material Fig. S3). Thus a portion of Shc-p52 pre-associates with ErbB family members in a phosphorylation-dependent (tyrosine kinase inhibitor-sensitive) manner and a further portion is recruited from the cytosol to receptors following a ligand-induced increase in phosphorylation. Shc-p46 plays no apparent role in ErbB signaling in SKBR3 cells.

PI 3-kinase is perhaps the most important binding partner of activated ErbB3 (Soltoff et al., 1994; Hellyer et al., 2001) and it is generally considered to be a poor binding partner for other ErbB receptors. The biochemical experiments in Fig. 5A show that a significant amount of p85 is pre-associated with crude membrane fractions and is not changed by treatment of cells with tyrosine kinase inhibitors. In addition, neither ligand significantly changes the ratio of p85 between membrane and cytosolic fractions. Fig. 5B examines the association of p85 with different receptors. Only anti-ErbB3 co-precipitates significant amounts of p85 from serum-starved cells (Fig. 5B). p85 is displaced from ErbB3 with tyrosine kinase inhibitors, indicating dependence on ErbB3 phosphorylation (see Fig. 5B). Addition of heregulin leads to a marked increase in p85 in ErbB3 immunoprecipitates.

Electron micrographs of membrane sheets prepared from resting cells show that most p85 is present in small clusters that are widely dispersed across the inner surface of the membrane, sometimes near ErbB3 (bold arrow, Fig. 5C) or along cable-like structures that may represent elements of the cortical cytoskeleton (small arrows, Fig. 5C). This image fails the Ripley's test for colocalization (supplementary material Fig. S3). After heregulin treatment, dramatic co-clustering of p85 with ErbB3 was often seen (encircled clusters in Fig. 5D). Colocalization was confirmed by the Ripley's test (see supplementary material Fig. S3). In addition, we observed novel bull's eye structures in these membranes (Fig. 5E), with ErbB3 clusters in the center (large gold particles) that are surrounded by heavy labeling of p85 (small gold particles). In this case, the downward projection of the red line in the Ripley's test indicates a strong deviation from normal (supplementary material Fig. S3). In summary, we see that PI 3-kinase is markedly recruited to ErbB3 clusters in activated cells, probably from the pool of inherently membrane-associated enzyme. Heregulin can also induce formation of a unique membrane domain around ErbB3 clusters that is distinguished here by a ring of PI 3-kinase.

Finally, Fig. 6 examines STAT5 association with the membranes of SKBR3 cells. Like Shc, STAT5 is a preferred binding partner of activated EGFR (Olayioye et al., 1999; Kloth et al., 2002). However, fractionation experiments (Fig. 6A) showed very little change in the overall levels of STAT5 in the membrane and cytosol fractions after EGF (or heregulin) treatment, and treatment with the tyrosine kinase inhibitor cocktail failed to displace STAT5 from the membrane. As expected, EGF led to phosphorylation of STAT5 within 30 seconds (Fig. 6C) and to the appearance of the phosphorylated STAT5 dimer in both the cytosolic and membrane fractions (Fig. 6A).

STAT5 co-precipitated with all three receptors, and EGF led to the appearance of a slightly slower migrating form, presumably representing phosphorylated STAT monomer (Fig. 6B). The persistent ability to co-precipitate STAT5 with all three receptors after treatment with tyrosine kinase inhibitor cocktail indicates that STAT5 association is not dependent upon receptor phosphorylation.

Membrane sheet experiments confirmed similar levels of STAT5 labeling on both resting and EGF-treated membranes (not shown), and documented that cell activation increased STAT5 phosphorylation. As shown in Fig. 6D, SKBR3 membranes prepared from serum-starved cells showed negligible binding of gold particles marking phospho-STAT5 (<11.8 particles per μm^2). After 2 minutes of EGF treatment (Fig. 6E), there was a dramatic increase in the amount of phospho-STAT5 labeled (>58.3 particles per μm^2). These results are also depicted in a bar graph in supplementary material Fig. S3. Double labeling experiments showed that this phospho-STAT5 was not preferentially associated with activated EGFR (Fig. 6F). In this micrograph, clusters of phospho-STAT5 and EGFR are marked with boxes, and the more abundant, dispersed clusters of phospho-STAT5 are encircled; this image fails the Ripley's test for co-clustering (supplementary material Fig. S3). Thus, STAT5 appears to associate inherently with ErbB isoforms and the principal effect of EGF appears to be the rapid tyrosine phosphorylation of pre-associated STAT5 and the redistribution of phospho-STAT5 to separate membrane microdomains.

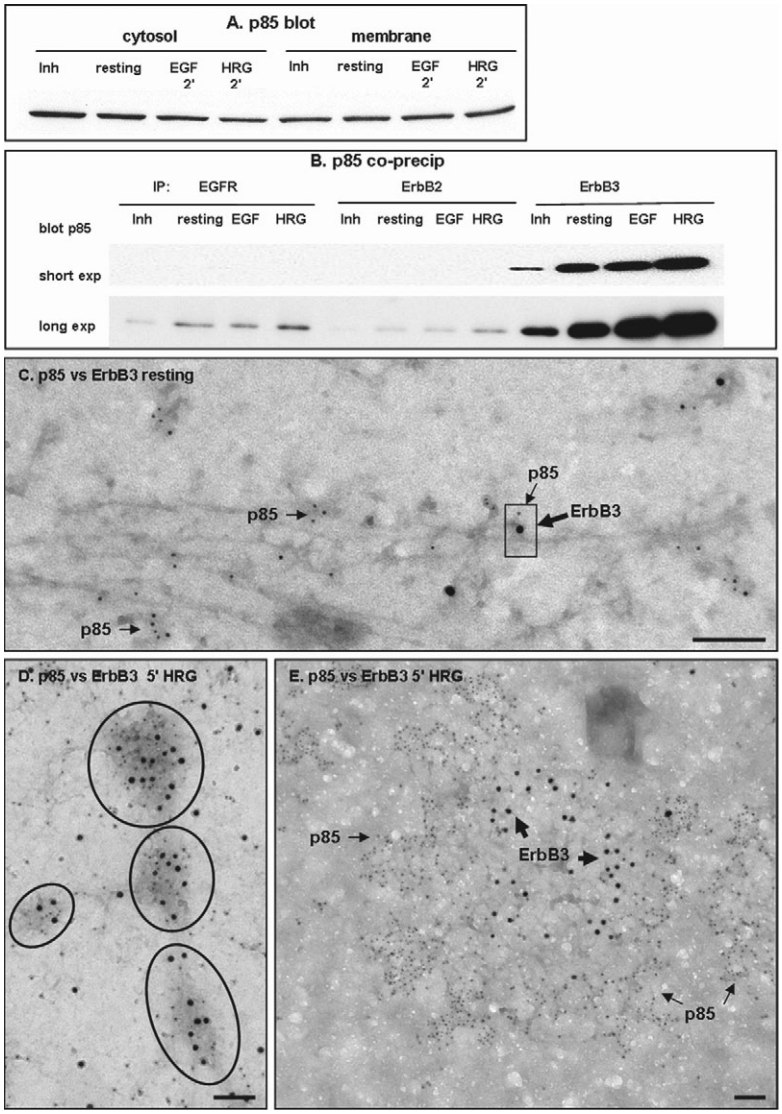

Fig. 5. Redistribution of membrane-associated PI 3-kinase in heregulin-stimulated SKBR3 cells. (A) Cytosol and membrane fractions were prepared from treated and untreated SKBR3 cells, as described in the legend to Fig. 4. Samples were subjected to SDS-PAGE and immunoblotting with anti-p85 antibodies. (B) Immunoblotting evidence for the co-precipitation of p85 with ErbB3 (and very little co-precipation with EGFR or ErbB2). Treatment of cells is indicated. Membrane sheets in C-E were prepared from serum starved cells (C) or cells treated for 5 minutes with 3.2 nm heregulin (D,E); membranes were then double labeled for p85 (5-nm gold) and ErbB3 (10-nm gold). Bold arrows in C and D point to labeled ErbB3 label and fine arrows to labeled p85 label. Circles in E indicate multiple co-clusters of ErbB3 and p85. Bars, 0.1 μm.

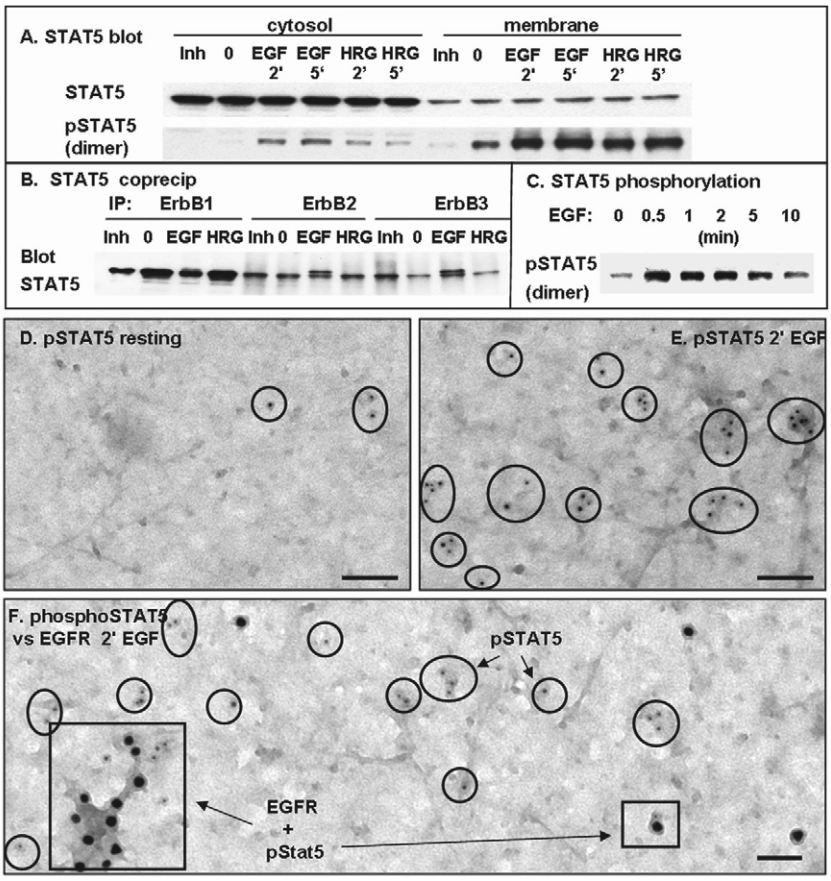

Fig. 6. Rapid tyrosine phosphorylation of membrane-associated STAT5 after treatment with EGF. (A) Cytosol and membrane fractions were prepared from treated and untreated SKBR3 cells, as described in the legend to Fig. 4. Samples were subjected to SDS-PAGE and immunoblotting with anti-STAT5 antibodies. (B) Immunoblotting evidence for the co-precipitation of STAT5 with EGFR and, to a lessor extent, to ErbB2/ErbB3. Treatment of cells is indicated. (C) Immunoblotting with anti-STAT5 PY694 antibodies demonstrates the time course of STAT5 phosphorylation in response to 20 nM EGF. Membrane sheets in D-F were prepared from serum starved SKBR3 cells (D) or after 2 minutes of treatment with 20 nM EGF (E,F). Sheets in E and D were singly labeled with 5-nm gold reagents that specifically recognize STAT5 when phosphorylated on Tyr694; there is marked increase in the amount of phospho-STAT5 (encircled) but not in the general pool of STAT5 after EGF treatment. The membrane sheet in F was double labeled for phospho-STAT5 (5-nm gold) and EGFR (10-nm gold). Boxed areas mark the few co-clusters of EGFR and phospho-STAT5 in EGF-treated membranes. Bars, 0.1 μm.

Discussion

Variability of ErbB receptor expression is considered to be an important factor in breast cancer prognosis (Rowinsky, 2004). Because dimerization is a key step in ErbB receptor activation, we propose that fine-scale membrane organization also contributes importantly to the oncogenic signaling process. We evaluated the spatial relationships of three family members (EGFR, ErbB2 and ErbB3), when expressed alone in transfected CHO cells and when co-expressed endogenously at high levels in a breast cancer line. This spatial information was acquired using immunoelectron microscopy of native membrane sheets, providing snapshots of receptors and their signaling partners at nanometer scale resolution.

We show that each of the ErbB receptors clusters independently when expressed in stably transfected CHO cells, even at very low expression levels. We observed large increases in cluster size for ErbB3 after ligand treatment but not in EGFR or ErbB2. EGF-induced changes in EGFR or ErbB2 cluster size have been reported by others using fluorescence microscopy techniques (Ichinose et al., 2004; Nagy et al., 1999). We suggest that differences in cell type, cell culture conditions and/or antibodies used to detect receptors may explain the discrepancy. In the course of these experiments, we ruled out the use of several commercial antibodies, originally raised against one ErbB family member but with significant crossreactivity to other ErbBs. This has been a subject of some controversy in the literature (DiGiovanna et al., 2005; Karlin et al., 2005). A few EGFR antibodies are also conformation-specific, which might lead to significant changes in labeling after EGF treatment (DiGiovanna, 1997; Johns et al., 2004).

It is significant that ErbB2 clusters are dominant features of the membrane in these breast cancer cells. ErbB2 is inherently clustered in resting cells and these clusters label with phospho-specific antibodies (Fig. 2). Since few ErbB2 clusters in serum-starved cells mix with other ErbB receptors, a high proportion of ErbB2 signaling must be driven by homo-interactions. We note that clustering is not dependent on phosphorylation because treatment with tyrosine kinase inhibitors does not change cluster size. We speculate that high densities of ErbB2 may drive dimer formation despite its reportably poor homodimerizing capability (Burgess et al., 2003).

The relatively low incidence of co-clustering between different ErbB receptors in resting cells suggests segregation as one mechanism to minimize premature formation of heterodimers, while potentially favoring rapid homodimerization of EGFR and ErbB3 upon treatment with their respective ligands. This is puzzling to consider for ErbB3, which is generally considered to be dependent upon heterodimerization with other ErbBs for initiation of signaling. Presently, we do not offer an explanation for the segregation of individual ErbB clusters. Possibilities include unique 'lipid shell' preferences for the individual receptor species (Anderson and Jacobson, 2002) or occupancy in different 'protein islands' (Lillemeier et al., 2006). Consistent with the latter hypothesis, most receptors occupy dark regions of the membrane that are a hallmark feature of the protein island hypothesis (Lillemeier et al., 2006). Another alternative is that clustering could be

mediated by weak homotypic interactions between the receptors themselves. Recent evidence suggests that ErbB3 can form 'conformationally inactive' oligomers through binding interactions that are distinct from the dimerization interface identified in crystal structures of the ligand-bound (extended) ErbBs (Kani et al., 2005). It has been estimated that up to 14% of EGFRs are oligomerized prior to growth factor binding (Martin-Fernandez et al., 2002). These oligomerized receptors may be autoinhibited through structural conformations, such as the electrostatic interaction of unphosphorylated tails with acidic lipids in the plasma membrane, a model proposed by McLaughlin and colleagues (McLaughlin et al., 2005).

The fact that we detect segregation in the crowded ErbB2 landscape is remarkable. Although co-clustering is not a direct measurement of dimerization, it is a direct measurement of proximity. We found that only 30% of the images double-labeled for EGFR and ErbB2 passed the Ripley's test for co-clustering. Thus, a majority of EGFR in EGF-stimulated SKBR3 cells are likely to be participating in homotypic, not heterotypic, interactions. Relevant to this argument, it has been suggested in previous studies that the heterodimerization of ligand-bound EGFR with ErbB2 results in a slower internalization rate for EGFR, possibly resulting in prolonged and aberrant signaling at the cell surface (Lidke et al., 2004; Wang et al., 1999).

We hypothesize that, under more normal expression levels, segregation may be a powerful tool to limit heterodimerization of EGFR and ErbB2. Our work also has important implications for computational models that attempt to predict biological outcomes in both normal and oncogenic settings. Most models have assumed EGFR-EGFR homodimers and EGFR-ErbB2 heterodimers are favored equally (Hendriks et al., 2003). In cells expressing over 2 million ErbB2 molecules, Hendricks'model predicts that >80% of ligand-bound EGFR occurs in heterodimers. If this were the case, essentially all EGFR clusters should also contain ErbB2. We did not observe this.

Docking partners, including Shc, PI 3-kinase and STAT5 are crucial for coupling growth factor signals to downstream activation pathways. Textbook models suggest that receptor phosphorylation results in recruitment of these partners from the cytoplasm and that dissociation occurs upon receptor dephosphorylation. Remarkably, none of the proteins studied here follow this model in detail. Shc-p52 is the closest. A portion of Shc-p52 pre-associates with all ErbB family members in a phosphorylation-dependent (tyrosine-kinase-inhibitor-sensitive) manner and a further portion is recruited from the cytosol to receptors following a ligand-induced increase in phosphorylation. PI 3-kinase deviates more strongly from the classic model. Heregulin strongly increases ErbB3-bound PI 3-kinase without appearing to increase total PI 3-kinases in membrane fractions. This suggests that the ErbB3-associated PI 3-kinase in activated cells derives mostly from a pool of inherently membrane-associated enzyme and not from the cytosol. STAT5 appears to associate inherently with EGFR and the principal effects of EGF appears to be the rapid tyrosine phosphorylation of pre-associated STAT5 and its redistribution to separate membrane microdomains. There is precedent for this unexpected topographical behavior in the case of LAT, a transmembrane protein of mast cells that is phosphorylated by Syk and immediately redistributes to membrane domains away from Syk and its partnering receptor FcεRI (Wilson et al., 2001).

The dramatic reorganization of ErbB3, together with PI 3-kinase, in heregulin-treated SKBR3 cells is of particular interest. Early studies in human mammary carcinomas (Alimandi et al., 1995) implicated the ErbB3/PI 3-kinase pathway as a crucial step in neoplastic transformation and a previous report using fluorescence imaging showed the first indications that the two signaling molecules co-patch on the cell surface (Gillham et al., 1999). We found that the formation of large ErbB3 complexes occurred over a somewhat slow time course (5 minutes), compared with the kinetics of receptor phosphorylation (peaks at 1-2 minutes; see Fig. 1). The large clusters of ErbB3 contained no visible clathrin structures, consistent with slow internalization. PI 3-kinase mixed readily with smaller ErbB3 clusters (Fig. 5E) and was also sometimes found within the larger ErbB3 clusters. However, it also was seen as a distinctive ring around large ErbB3 clusters (Fig. 5D). Because the other ErbBs are neither recruited into nor restricted from the large ErbB3 clusters, we assume that the unique spatial relationships between ErbB3 and p85 is dynamic and not restricted by a corral (Tomishige et al., 1998). It is likely to only be incidentally similar to the immunological synapse that also forms a bull's eye (Bromley et al., 2001). The p85 that associates with activated ErbB3 appears to derive from a membrane-associated pool. Further study is needed to identify the binding sites involved in anchoring p85 to the membrane in resting cells.

In summary, high-resolution imaging has documented several unique aspects of ErbB signaling. Most notably, we implicate segregation of ErbB family members as a potential way to limit heterodimerization to levels much lower than currently predicted. The discovery of three distinct membrane recruitment and topographical patterns for specific signaling proteins associated with ErbB signal propagation, none exactly following the conventional model, needs to be considered in future models of growth factor signaling in the context of breast cancer and other cancers.

Materials and Methods

Cell lines

SKBR3 cells were obtained from ATCC and grown according to guidelines. CHO cells stably transfected with EGFR-GFP, erbB2-mYFP or erbB3-mCitrine (Lidke et al., 2004) were gifts from Thomas M. Jovin and Donna Arndt-Jovin (Max Planck Institute, Göttingen, Germany). CHO cells were cultured in DMEM, 10% FBS (Hyclone) with penicillin-streptomycin and L-glutamine.

Reagents

Epidermal growth factor (EGF) was from Biomedical Technologies (Stoughton, MA). Recombinant heregulin β was from US Biological (Swampscott, MA). AG1478 was from Alexis Biochemicals (San Diego, CA); AG879, PD153035, PP2 and staurosporin were from Calbiochem (LA, Jolla, CA). EGFR-specific antibodies were EGFR.1 (Calbiochem, La Jolla, CA) and 610016 (BD Transduction Laboratories). ErbB2-specific antibodies were RB9040 (Labvision), SC-08 (Santa Cruz Biotechnology, CA) and MS-325 (Labvision). Anti-ErbB3 SC-285 and SC-415 antibodies, p85 SC-423 antibodies and STAT5 SC-838 antibodies were also from Santa Cruz. Anti-Shc 610081 antibodies were from BD Transduction. Anti-p85 06-497 antibodies were from UBI (Lake Placid, NY). Antibodies against phospho694 STAT5 and phospho-ErbBs, were from Cell Signaling. HRP-conjugated PY20 was from BD Transduction Laboratories.

Western blotting and immunoprecipitation analysis

Cells were serum-starved (2 hours) then stimulated with ligands. After a PBS rinse, cells were solubilized in cold NP-40 lysis buffer (150 mM NaCl, 50 mM Tris/HCl pH 7.2, 1% NP-40, 5 μg/ml leupeptin, 5 μg/ml antipain, 1 mM $NaVO_4$, 1 mM PMSF). Lysates were clarified by centrifugation. Protein concentrations were measured by BCA protein assay (Pierce). Supernatants were mixed with 5× sample buffer for SDS-PAGE or used directly for immunoprecipitations. For IP, supernatants were preincubated with Trueblot anti-mouse or anti-rabbit Ig beads

(Ebioscience, San Diego, CA), followed by transfer to tubes containing specific antibodies and overnight incubation at 4°C. After four washes in lysis buffer, 2× reducing Laemmli buffer was added to beads for SDS-PAGE and subsequent transfer to nitrocellulose membranes. Blocked membranes were probed with primary and HRP-conjugated secondary antibodies, followed by detection of bands by ECL (Pierce).

Cytosol and membrane fractionation

Cells were serum starved for 2 hours and, where indicated, inhibitors were added for the last hour prior to addition of agonist. Cells were transferred to 4°C, rinsed with PBS, scraped off and briefly sonicated; intact cells and debris were sedimented by microcentrifugation (10 minutes). Cloudy supernatants were subjected to ultracentrifugation (100,000 ***g***, 1 hour, 4°C) to yield membrane and cytosol fractions. Membrane pellets were dissolved in cold NP-40 lysis buffer. Protein concentrations in fractions were determined by BCA assay to normalize samples prepared for SDS-PAGE.

In vitro tyrosine kinase assays

K-LISA EAY kits (Calbiochem, La Jolla, CA) were used to measure kinase activity in receptor immunoprecipitates. Receptors were immunoprecipitated (using EGFR.1 for EGFR or RB9040 for ErbB2) and aliquots of precipitate-slurry transferred to replicate wells of K-LISA strips. Strips were incubated with and without inhibitors, washed and read on a spectrofluorimeter, according to the manufacturer's protocol.

Flow cytometry to quantify surface expression of EGFR, ErbB2 and ErbB3

Cells were detached with Tris-EDTA/PBS (Sigma) and labeled for 1 hour at 4°C with saturating amounts of FITC-conjugated antibodies against EGFR (sc-120 FITC), ErbB2 (sc-23864 FITC) or ErbB3 (sc-23865 FITC). Calibration beads (Quantum Simply Cellular, Anti-Mouse IgG, Banglabs, Fishers, IN) were labeled in parallel for each condition. After PBS rinses, samples and beads were analyzed by FACScan (BD Bioscience). Receptor numbers were determined using the calibration curve generated from the bead standards.

Preparation of plasma membrane sheets and gold labeling for TEM

Detailed methods are described in earlier papers (Wilson et al., 2000; Wilson et al., 2001; Wilson et al., 2004). A recent chapter (Wilson et al., 2007) reports both FRAP and single-particle-tracking experiments, demonstrating that PFA fixation immobilizes membrane proteins prior to labeling. In brief, cells were cultured on 15-mm round, clean glass coverslips. After incubation at 37°C with or without stimuli, cells on coverslips were fixed in 0.5-2% PFA (10 minutes, room temperature), inverted onto EM grids and ripped. The stronger (2% PFA) fix was used when cells were prelabeled from the outside with immunogold reagents. In all cases, EM grids were incubated in 2% PFA for an additional 20 minutes after ripping. Grids were glow-discharged and coated with formvar and poly-L-lysine. Washed membranes were labeled from the inside by incubating sequentially with primary antibodies and gold-conjugated secondary reagents. Sheets were post-fixed with 2% glutaraldehyde (20 minutes, room temperature), stained with tannic acid and uranyl acetate and digital images acquired on an Hitachi H-7500 transmission electron microscope. At least ten images were taken from at least two separate experiments for each condition.

Mapping and analysis of gold particle distribution

Digital images (6.8 megapixels) were analyzed using a customized ImageJ plugin to find and count coordinates of 5 and 10 nm particles automatically (Zhang et al., 2005). Coordinates were analyzed using the Hopkins test for clustering (Jain and Dubes, 1988; Wilson et al., 2004; Zhang et al., 2005). The Ripley's K bivariate function was used to evaluate co-clustering (Haase, 1995; Wilson et al., 2004; Zhang et al., 2005). Markov random field simulations were used to account for hidden receptors (Zhang et al., 2007).

This work was supported by NIH grants R01 CA119232 (B.W.) and P20 GM067594 (J.M.O.) and by the Oxnard Foundation (B.W.). J.Z. was a Gies Foundation fellow, UNM CRTC. Use of the EM and flow cytometry facilities at the UNM SOM and CRTC, and NIH support for these cores, is gratefully acknowledged. Spatial statistics tools used here are available at http://cellpath.health.unm.edu/stmc/emtools/index.html.

References

Alimandi, M., Romano, A., Curia, M. C., Muraro, R., Fedi, P., Aaronson, S. A., Di Fiore, P. P. and Kraus, M. H. (1995). Cooperative signaling of ErbB3 and ErbB2 in neoplastic transformation and human mammary carcinomas. *Oncogene* **10**, 1813-1821.

Anderson, R. G. and Jacobson, K. (2002). A role for lipid shells in targeting proteins to caveolae, rafts, and other lipid domains. *Science* **296**, 1821-1825.

Bouyain, S., Longo, P. A., Li, S., Ferguson, K. M. and Leahy, D. J. (2005). The extracellular region of ErbB4 adopts a tethered conformation in the absence of ligand. *Proc. Natl. Acad. Sci. USA* **102**, 15024-15029.

Bromley, S. K., Burack, W. R., Johnson, K. G., Somersalo, K., Sims, T. N., Sumen, C., Davis, M. M., Shaw, A. S., Allen, P. M. and Dustin, M. L. (2001). The immunological synapse. *Annu. Rev. Immunol.* **19**, 375-396.

Burgess, A. W., Cho, H. S., Eigenbrot, C., Ferguson, K. M., Garrett, T. P., Leahy, D. J., Lemmon, M. A., Sliwkowski, M. X., Ward, C. W. and Yokoyama, S. (2003). An open-and-shut case? Recent insights into the activation of EGF/ErbB receptors. *Mol. Cell* **12**, 541-552.

DiGiovanna, M. P. (1997). Phosphorylation sensitivity of the commonly used anti-p185neu/erbB2 monoclonal antibody clone 3B5 suggests selective usage of autophosphorylation sites. *Anal. Biochem.* **247**, 167-170.

DiGiovanna, M. P., Stern, D. F., Edgerton, S. M., Whalen, S. G., Moore, D., 2nd and Thor, A. D. (2005). Relationship of epidermal growth factor receptor expression to ErbB-2 signaling activity and prognosis in breast cancer patients. *J. Clin. Oncol.* **23**, 1152-1160.

Garrett, T. P., McKern, N. M., Lou, M., Elleman, T. C., Adams, T. E., Lovrecz, G. O., Kofler, M., Jorissen, R. N., Nice, E. C., Burgess, A. W. et al. (2003). The crystal structure of a truncated ErbB2 ectodomain reveals an active conformation, poised to interact with other ErbB receptors. *Mol. Cell* **11**, 495-505.

Gillham, H., Golding, M. C., Pepperkok, R. and Gullick, W. J. (1999). Intracellular movement of green fluorescent protein-tagged phosphatidylinositol 3-kinase in response to growth factor receptor signaling. *J. Cell Biol.* **146**, 869-880.

Guy, P. M., Platko, J. V., Cantley, L. C., Cerione, R. A. and Carraway, K. L., 3rd (1994). Insect cell-expressed p180erbB3 possesses an impaired tyrosine kinase activity. *Proc. Natl. Acad. Sci. USA* **91**, 8132-8136.

Haase, P., (1995). Spatial pattern analysis in ecology based on ripley's K function: introduction and methods of edge correction. Journal of Vegetation Science 6, 575-582.

Harari, D. and Yarden, Y. (2000). Molecular mechanisms underlying ErbB2/HER2 action in breast cancer. *Oncogene* **19**, 6102-6114.

Hellyer, N. J., Kim, M. S. and Koland, J. G. (2001). Heregulin-dependent activation of phosphoinositide 3-kinase and Akt via the ErbB2/ErbB3 co-receptor. *J. Biol. Chem.* **276**, 42153-42161.

Hendriks, B. S., Opresko, L. K., Wiley, H. S. and Lauffenburger, D. (2003). Quantitative analysis of HER2-mediated effects on HER2 and epidermal growth factor receptor endocytosis: distribution of homo- and heterodimers depends on relative HER2 levels. *J. Biol. Chem.* **278**, 23343-23351.

Huang, F., Khvorova, A., Marshall, W. and Sorkin, A. (2004). Analysis of clathrin-mediated endocytosis of epidermal growth factor receptor by RNA interference. *J. Biol. Chem.* **279**, 16657-16661.

Ichinose, J., Murata, M., Yanagida, T. and Sako, Y. (2004). EGF signalling amplification induced by dynamic clustering of EGFR. *Biochem. Biophys. Res. Commun.* **324**, 1143-1149.

Jain. A.K. and Dubes, R.C. (1988) *Algorithms for clustering data advanced reference series*. Prentice-Hall, Englewood Cliffs, NJ.

Johns, T. G., Adams, T. E., Cochran, J. R., Hall, N. E., Hoyne, P. A., Olsen, M. J., Kim, Y. S., Rothacker, J., Nice, E. C., Walker, F. et al. (2004). Identification of the epitope for the epidermal growth factor receptor-specific monoclonal antibody 806 reveals that it preferentially recognizes an untethered form of the receptor. *J. Biol. Chem.* **279**, 30375-30384.

Jorissen, R. N., Walker, F., Pouliot, N., Garrett, T. P., Ward, C. W. and Burgess, A. W. (2003). Epidermal growth factor receptor: mechanisms of activation and signalling. *Exp. Cell Res.* **284**, 31-53.

Kani, K., Warren, C. M., Kaddis, C. S., Loo, J. A. and Landgraf, R. (2005). Oligomers of ERBB3 have two distinct interfaces that differ in their sensitivity to disruption by heregulin. *J. Biol. Chem.* **280**, 8238-8247.

Karlin, J. D., Nguyen, D., Yang, S. X. and Lipkowitz, S. (2005). Epidermal growth factor receptor expression in breast cancer. *J. Clin. Oncol.* **23**, 8118-8119; author reply 8119-8120.

Kim, J. H., Cramer, L., Mueller, H., Wilson, B. and Vilen, B. J. (2005). Independent trafficking of Ig-alpha/Ig-beta and mu-heavy chain is facilitated by dissociation of the B cell antigen receptor complex. *J. Immunol.* **175**, 147-154.

Kloth, M. T., Catling, A. D. and Silva, C. M. (2002). Novel activation of STAT5b in response to epidermal growth factor. *J. Biol. Chem.* **277**, 8693-8701.

Koleske, A. J., Baltimore, D. and Lisanti, M. P. (1995). Reduction of caveolin and caveolae in oncogenically transformed cells. *Proc. Natl. Acad. Sci. USA* **92**, 1381-1385.

Kraus, M. H., Popescu, N. C., Amsbaugh, S. C. and King, C. R. (1987). Overexpression of the EGF receptor-related proto-oncogene erbB-2 in human mammary tumor cell lines by different molecular mechanisms. *EMBO J.* **6**, 605-610.

Lidke, D. S., Nagy, P., Heintzmann, R., Arndt-Jovin, D. J., Post, J. N., Grecco, H. E., Jares-Erijman, E. A. and Jovin, T. M. (2004). Quantum dot ligands provide new insights into erbB/HER receptor-mediated signal transduction. *Nat. Biotechnol.* **22**, 198-203.

Lillemeier, B. F., Pfeiffer, J. R., Surviladze, Z., Wilson, B. S. and Davis, M. M. (2006). Plasma membrane-associated proteins are clustered into islands attached to the cytoskeleton. *Proc. Natl. Acad. Sci. USA* **103**, 18992-18997.

Martin-Fernandez, M., Clarke, D. T., Tobin, M. J., Jones, S. V. and Jones, G. R. (2002). Preformed oligomeric epidermal growth factor receptors undergo an ectodomain structure change during signaling. *Biophys. J.* **82**, 2415-2427.

McLaughlin, S., Smith, S. O., Hayman, M. J. and Murray, D. (2005). An electrostatic

engine model for autoinhibition and activation of the epidermal growth factor receptor (EGFR/ErbB) family. *J. Gen. Physiol.* **126**, 41-53.

Mineo, C., Gill, G. N. and Anderson, R. G. (1999). Regulated migration of epidermal growth factor receptor from caveolae. *J. Biol. Chem.* **274**, 30636-30643.

Nagy, P., Jenei, A., Kirsch, A. K., Szollosi, J., Damjanovich, S. and Jovin, T. M. (1999). Activation-dependent clustering of the erbB2 receptor tyrosine kinase detected by scanning near-field optical microscopy. *J. Cell Sci.* **112**, 1733-1741.

Nagy, P., Vereb, G., Sebestyen, Z., Horvath, G., Lockett, S. J., Damjanovich, S., Park, J. W., Jovin, T. M. and Szollosi, J. (2002). Lipid rafts and the local density of ErbB proteins influence the biological role of homo- and heteroassociations of ErbB2. *J. Cell Sci.* **115**, 4251-4262.

Olayioye, M. A., Beuvink, I., Horsch, K., Daly, J. M. and Hynes, N. E. (1999). ErbB receptor-induced activation of stat transcription factors is mediated by Src tyrosine kinases. *J. Biol. Chem.* **274**, 17209-17218.

Orr, G., Hu, D., Ozcelik, S., Opresko, L. K., Wiley, H. S. and Colson, S. D. (2005). Cholesterol dictates the freedom of EGF receptors and HER2 in the plane of the membrane. *Biophys. J.* **89**, 1362-1373.

Penuel, E., Akita, R. W. and Sliwkowski, M. X. (2002). Identification of a region within the ErbB2/HER2 intracellular domain that is necessary for ligand-independent association. *J. Biol. Chem.* **277**, 28468-28473.

Pike, L. J., Han, X. and Gross, R. W. (2005). Epidermal growth factor receptors are localized to lipid rafts that contain a balance of inner and outer leaflet lipids: a shotgun lipidomics study. *J. Biol. Chem.* **280**, 26796-26804.

Prior, I. A., Muncke, C., Parton, R. G. and Hancock, J. F. (2003). Direct visualization of Ras proteins in spatially distinct cell surface microdomains. *J. Cell Biol.* **160**, 165-170.

Puri, C., Tosoni, D., Comai, R., Rabellino, A., Segat, D., Caneva, F., Luzzi, P., Di Fiore, P. P. and Tacchetti, C. (2005). Relationships between EGFR signaling-competent and endocytosis-competent membrane microdomains. *Mol. Biol. Cell* **16**, 2704-2718.

Ringerike, T., Blystad, F. D., Levy, F. O., Madshus, I. H. and Stang, E. (2002). Cholesterol is important in control of EGF receptor kinase activity but EGF receptors are not concentrated in caveolae. *J. Cell Sci.* **115**, 1331-1340.

Roepstorff, K., Thomsen, P., Sandvig, K. and van Deurs, B. (2002). Sequestration of epidermal growth factor receptors in non-caveolar lipid rafts inhibits ligand binding. *J. Biol. Chem.* **277**, 18954-18960.

Roskoski, R., Jr (2004). The ErbB/HER receptor protein-tyrosine kinases and cancer. *Biochem. Biophys. Res. Commun.* **319**, 1-11.

Rowinsky, E. K. (2004). The erbB family: targets for therapeutic development against cancer and therapeutic strategies using monoclonal antibodies and tyrosine kinase inhibitors. *Annu. Rev. Med.* **55**, 433-457.

Schulze, W. X., Deng, L. and Mann, M. (2005). Phosphotyrosine interactome of the ErbB-receptor kinase family. *Mol. Syst. Biol.* **1**, PMID: 16729043.

Sierke, S. L., Cheng, K., Kim, H. H. and Koland, J. G. (1997). Biochemical characterization of the protein tyrosine kinase homology domain of the ErbB3 (HER3) receptor protein. *Biochem. J.* **322**, 757-763.

Smart, E. J., Ying, Y. S., Mineo, C. and Anderson, R. G. (1995). A detergent-free method for purifying caveolae membrane from tissue culture cells. *Proc. Natl. Acad. Sci. USA* **92**, 10104-10108.

Soltoff, S. P., Carraway, K. L., 3rd, Prigent, S. A., Gullick, W. G. and Cantley, L. C. (1994). ErbB3 is involved in activation of phosphatidylinositol 3-kinase by epidermal growth factor. *Mol. Cell. Biol.* **14**, 3550-3558.

Tikhomirov, O. and Carpenter, G. (2004). Ligand-induced, p38-dependent apoptosis in cells expressing high levels of epidermal growth factor receptor and ErbB-2. *J. Biol. Chem.* **279**, 12988-12996.

Tomishige, M., Sako, Y. and Kusumi, A. (1998). Regulation mechanism of the lateral diffusion of band 3 in erythrocyte membranes by the membrane skeleton. *J. Cell. Biol.* **142**, 989-1000.

Wang, Z., Zhang, L., Yeung, T. K. and Chen, X. (1999). Endocytosis deficiency of epidermal growth factor (EGF) receptor-ErbB2 heterodimers in response to EGF stimulation. *Mol. Biol. Cell* **10**, 1621-1636.

Warren, C. M. and Landgraf, R. (2006). Signaling through ERBB receptors: multiple layers of diversity and control. *Cell. Signal.* **18**, 923-933.

Wilson, B. S., Pfeiffer, J. R. and Oliver, J. M. (2000). Observing FcepsilonRI signaling from the inside of the mast cell membrane. *J. Cell Biol.* **149**, 1131-1142.

Wilson, B. S., Pfeiffer, J. R., Surviladze, Z., Gaudet, E. A. and Oliver, J. M. (2001). High resolution mapping of mast cell membranes reveals primary and secondary domains of Fc(epsilon)RI and LAT. *J. Cell Biol.* **154**, 645-658.

Wilson, B. S., Steinberg, S. L., Liederman, K., Pfeiffer, J. R., Surviladze, Z., Zhang, J., Samelson, L. E., Yang, L. H., Kotula, P. G. and Oliver, J. M. (2004). Markers for detergent-resistant lipid rafts occupy distinct and dynamic domains in native membranes. *Mol. Biol. Cell* **15**, 2580-2592.

Wilson, B. S., Pfeiffer, J. R., Raymond-Stintz, M., Lidke, D., Lidke, K., Andrews, N. and Oliver, J. M. (2007). Electron microscopy methods to study membrane organization. In *Methods in Molecular Biology* Vol. 398 (ed. T. McIntosh). pp, 247-263, Humana Press.

Yarden, Y. and Sliwkowski, M. X. (2001). Untangling the ErbB signalling network. *Nat. Rev. Mol. Cell Biol.* **2**, 127-137.

Zhang, Y., Wolf-Yadlin, A., Ross, P. L., Pappin, D. J., Rush, J., Lauffenburger, D. A. and White, F. M. (2005). Time-resolved mass spectrometry of tyrosine phosphorylation sites in the epidermal growth factor receptor signaling network reveals dynamic modules. *Mol. Cell. Proteomics* **4**, 1240-50.

Zhang, J., Steinberg, S., Wilson, B. S., Oliver, J. M. and Williams, L. (2007). Markov random field modeling of the spatial distribution of proteins on cell membranes. *Bull. Math. Biol.* (*in press*).